SI: Decoupling the shape parameter to assess gold nanorod uptake by mammalian cells

C. Kinnear,[a,b] L. Rodriguez-Lorenzo,[a] M. J. D. Clift,[a,c] B. Goris,[d] S. Bals,[d] B. Rothen-Rutishauser,[a] and A. Petri-Fink[a,e]

[a.] *Adolphe Merkle Institute, University of Fribourg, Fribourg 1700, Switzerland.*
[b.] *Present address: School of Chemistry and Bio21 Institute, University of Melbourne, Victoria, Australia.*
[c.] *Present address: In Vitro Toxicology Group, Swansea University Medical School. Singleton Park Campus, Swansea, SA2 8PP, Wales, United Kingdom*
[d.] *Electron Microscopy for Materials Research (EMAT), University of Antwerp, Antwerp 2020, Belgium.*

Table of Contents

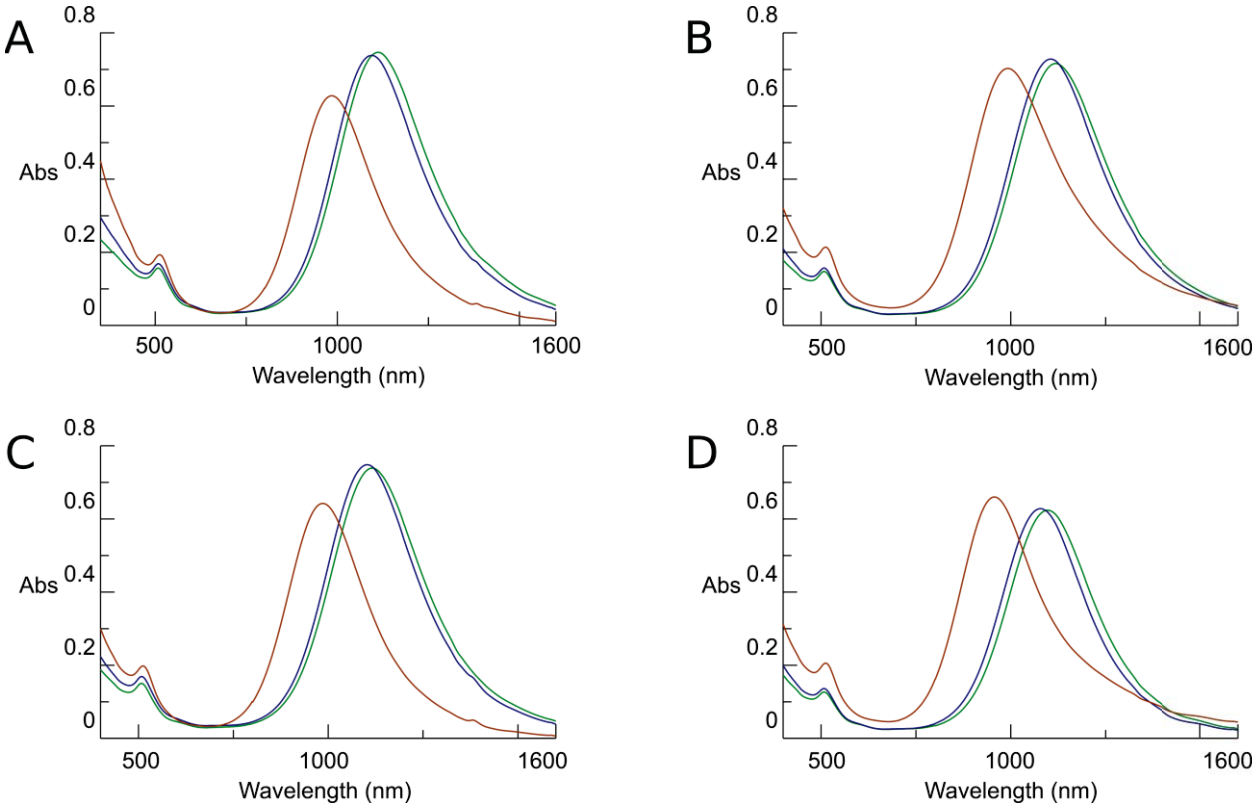

Fig. S1. Thermal reshaping at high PVP concentrations. Vis-NIR spectra of aliquots of PVP coated GNRs dispersed in DMF, upon heating to 140 °C, at 10 min (green line), 20 min (blue line), and 60 min (red line). The concentration of PVP was held constant at 5 mM while the concentration of CTAB was varied: (*A*) 0.3 mM, (*B*) 0.8 mM, (*C*) 1.6 mM, and (*D*) 2.9 mM.

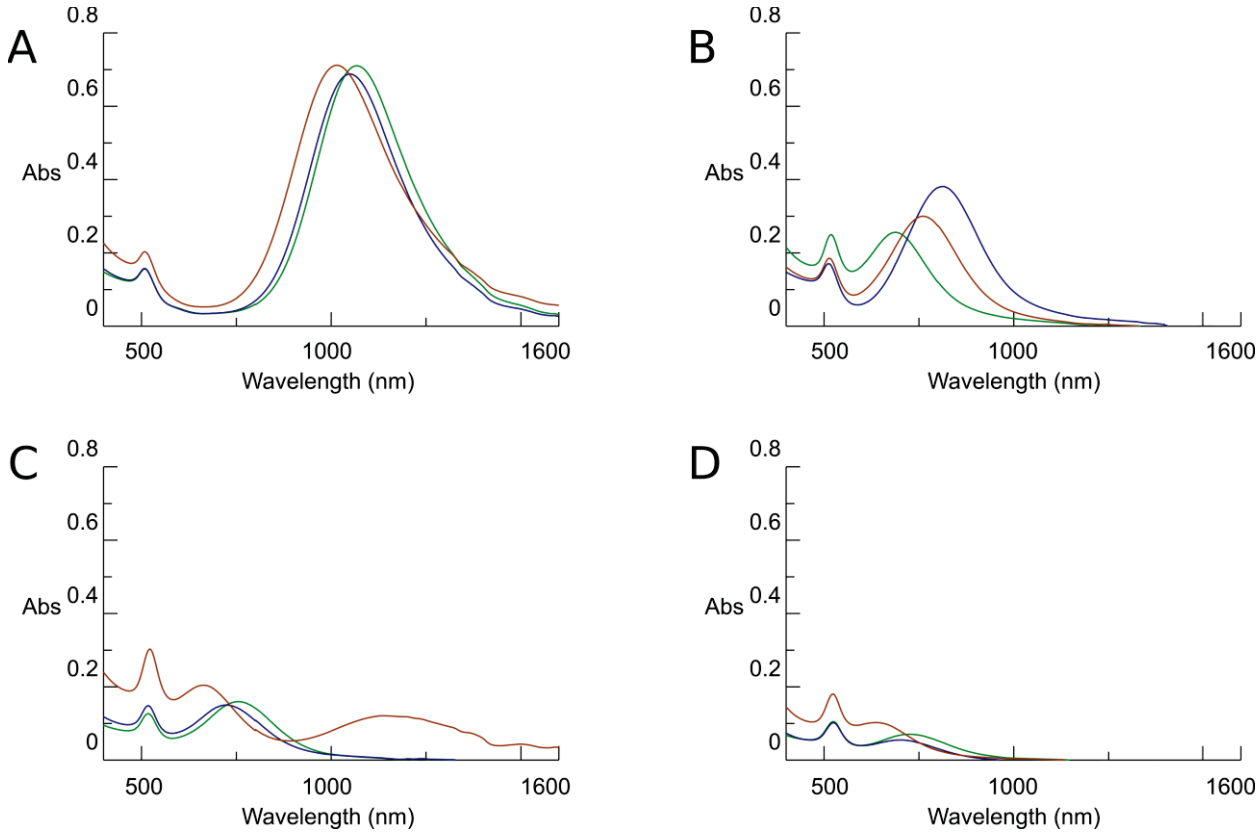

Fig. S2. Thermal reshaping at low PVP concentrations. Vis-NIR spectra of aliquots of PVP coated GNRs dispersed in DMF, upon heating to 140 °C, at 10 min (green line), 20 min (blue line), and 60 min (red line). The concentration of PVP was held constant at 1 mM while the concentration of CTAB was varied: (*A*) 0.3 mM, (*B*) 0.8 mM, (*C*) 1.6 mM, and (*D*) 2.9 mM.

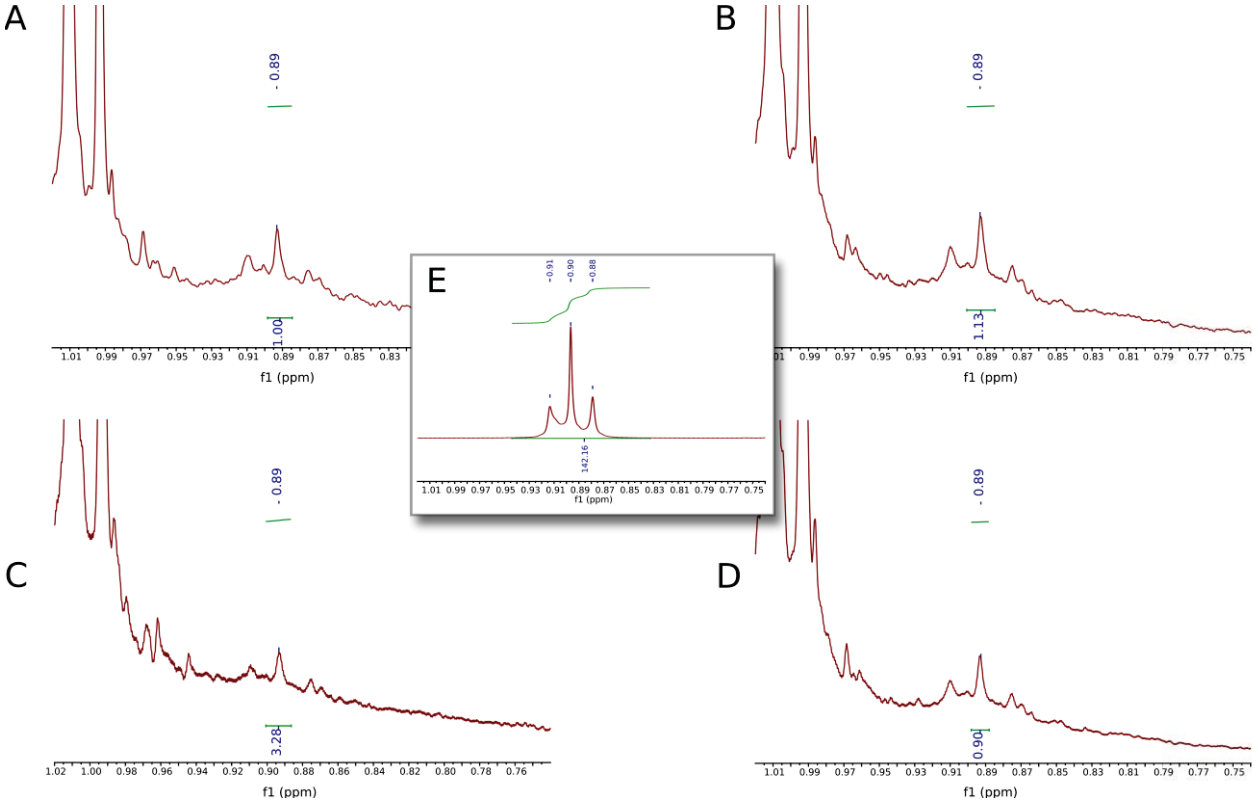

Fig. S3. ^{1}H NMR identifying surface adsorbed CTAB. ^{1}H NMR of residual CTAB identified through triplet at 0.89 ppm after dissolution of gold core by iodine in deuterated methanol (*A*) GNR-7.2, (*B*) GNR-4.8, (*C*) GNR-2.6, (*D*) GNR-1.9, and pure compound in deuterated methanol (*E*) CTAB (11.8 mM). The integrals are relative to the integral of the tetramethylsilane reference at 0 ppm normalized to 100.

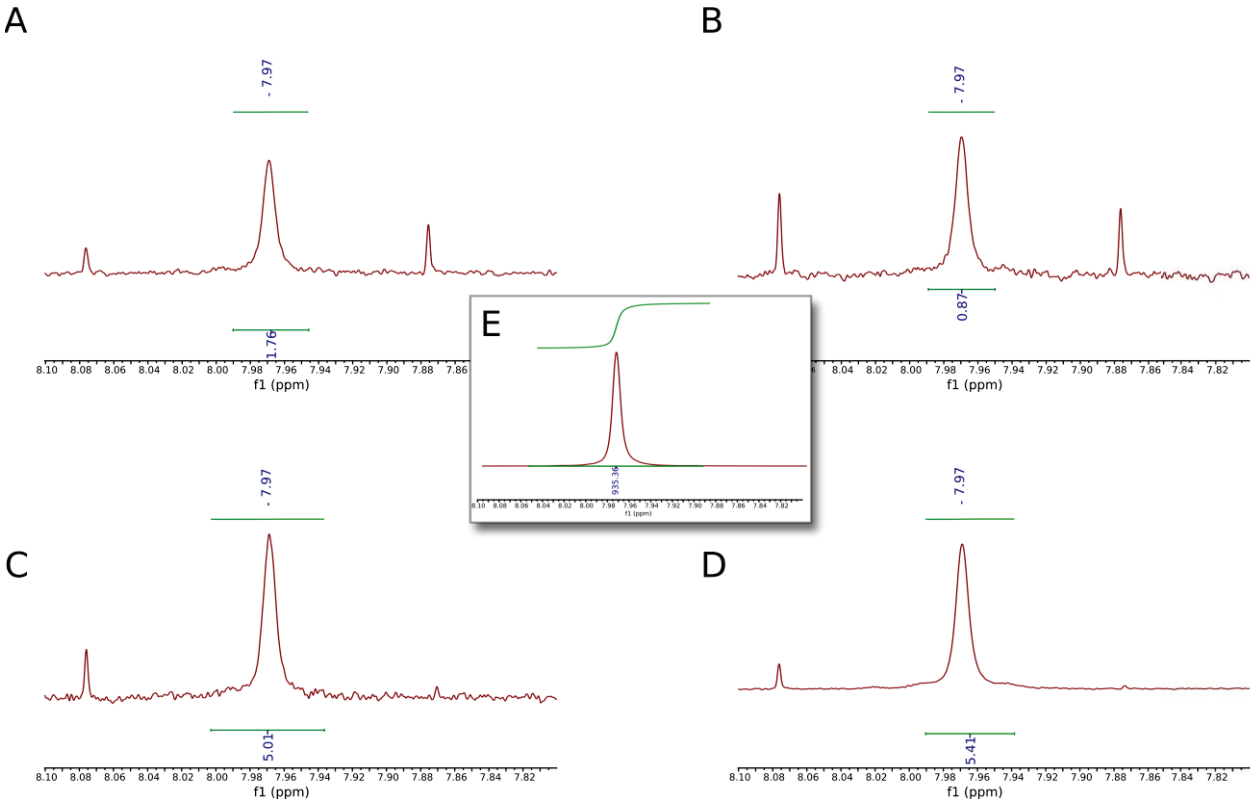

Fig. S4. ^{1}H NMR identifying surface adsorbed DMF. ^{1}H NMR of residual DMF identified through singlet at 7.98 ppm after dissolution of gold core by iodine in deuterated methanol (*A*) GNR-7.2, (B) GNR-4.8, (*C*) GNR-2.6, (*D*) GNR-1.9, and pure compound in deuterated methanol (*E*) DMF (1.7 vol. %). The integrals are relative to the integral of the tetramethylsilane reference at 0 ppm normalized to 100.

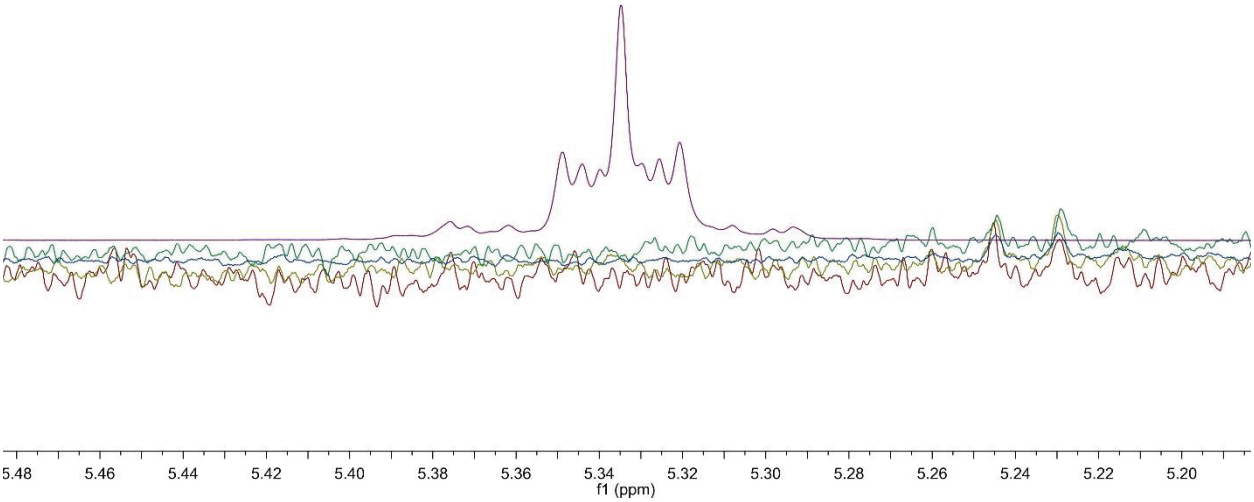

Fig. S5. ^{1}H NMR identifying surface adsorbed sodium oleate. ^{1}H NMR of residual sodium oleate after dissolution of gold core by iodine in deuterated methanol (red) GNR-7.2, (yellow) GNR-4.8, (green) GNR-2.6, (blue) GNR-1.9, and pure compound in deuterated methanol (purple) sodium oleate (57 mM). The scale of the four GNR samples has been increased by a factor of 10,000 relative to the sodium oleate control.

Table S1. Concentration of ligands. Summary of concentrations estimated via semi-quantitative ^{1}H NMR of reshaped and dissolved GNRs in deuterated methanol.

Sample	CTAB (μM)	DMF (vol. %)	PVP (mM)	NaOL
GNR-7.2	0.07	0.02	1.1	0
GNR-4.8	0.09	0.01	1.2	0
GNR-2.6	0.18	0.05	2.2	0
GNR-1.9	0.06	0.06	1.5	0

Table S2. Characterization of GNRs. Zeta-potential of reshaped GNRs dispersed in 0.1x PBS; the standard deviation is from three repeated measurements. The diffusion coefficient was measured by nanoparticle tracking analysis (NTA) and depolarized dynamic light scattering (DDLS) whereby a spherical hydrodynamical model was used to approximate the hydrodynamic radius (R_H) of the nanorods from the measured translational diffusion coefficients via the Stokes-Einstein relation.

Sample	Zeta-potential (mV)	R_H (nm) from NTA	R_H (nm) from DDLS
GNR-7.2	-7.2 ± 2.6	38 ± 1	37
GNR-4.8	-5.7 ± 1.1	37 ± 1	35
GNR-2.6	-15.0 ± 1.4	34 ± 1	34
GNR-1.9	-13.2 ± 1.7	31 ± 1	38

Table S3. Physical dimensions of reshaped GNRs from low resolution TEM. The length and width of at least 450 nanoparticles were measured via TEM, with either a spherocylindrical or spherical model used to calculate the mean volume and surface area based on whether the nanoparticle was a rod or a sphere. The number concentration was measured via nanoparticle tracking analysis of diluted samples where the mass concentration was held constant across samples, as identified by ICP-OES. The detection threshold, within the proprietary Nanosight software, was left unchanged between samples enabling an approximate comparison.

Measurement	GNR-7.2	GNR-4.8	GNR-2.6	GNR-1.9
Dimensions (nm)	113 × 16	84 × 18	62 × 24	55 × 29
Aspect Ratio	7.2	4.8	2.6	1.9
Volume (nm3)	22,800 ± 600	20,100 ± 530	22,400 ± 460	22,700 ± 440
Surface Area (nm2)	5,534 ± 210	4,629 ± 72	4,254 ± 69	3,952 ± 57
Shape Yield	90%	94%	81%	55%
Concentration from nanoparticle tracking analysis ($\times 10^8$ GNR.mL^{-1})	6.69 ± 0.41	6.37 ± 0.40	7.35 ± 0.23	7.94 ± 0.30

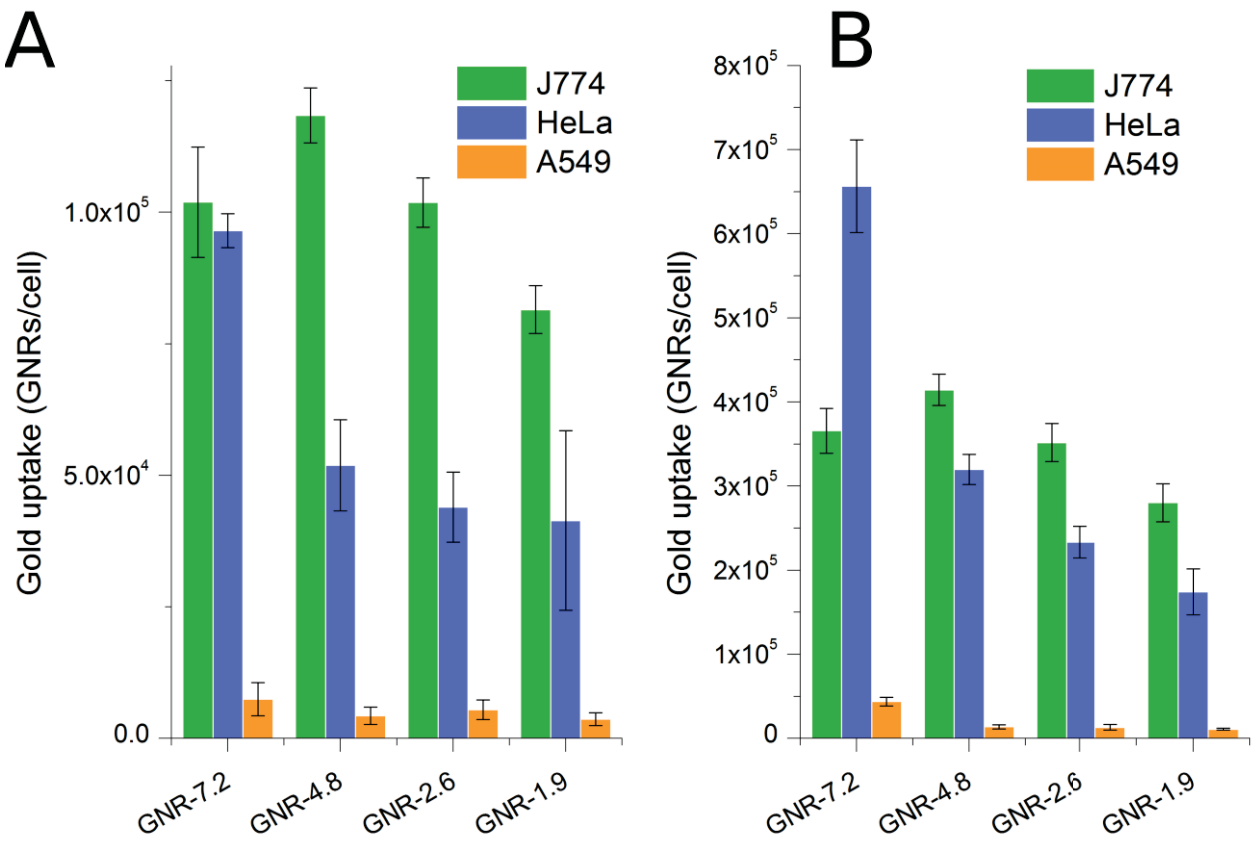

Fig. S6. Quantity of endocytosed gold nanorods per cell. Intracellular gold measured by ICP-OES in cell lysate after iodine wash to remove extracellular GNRs, expressed relative to the number of cells seeded. Three different cell lines were incubated with PVP coated reshaped GNRs at 40 μg.mL^{-1} for either 4 h (*A*) or 24 h (*B*).

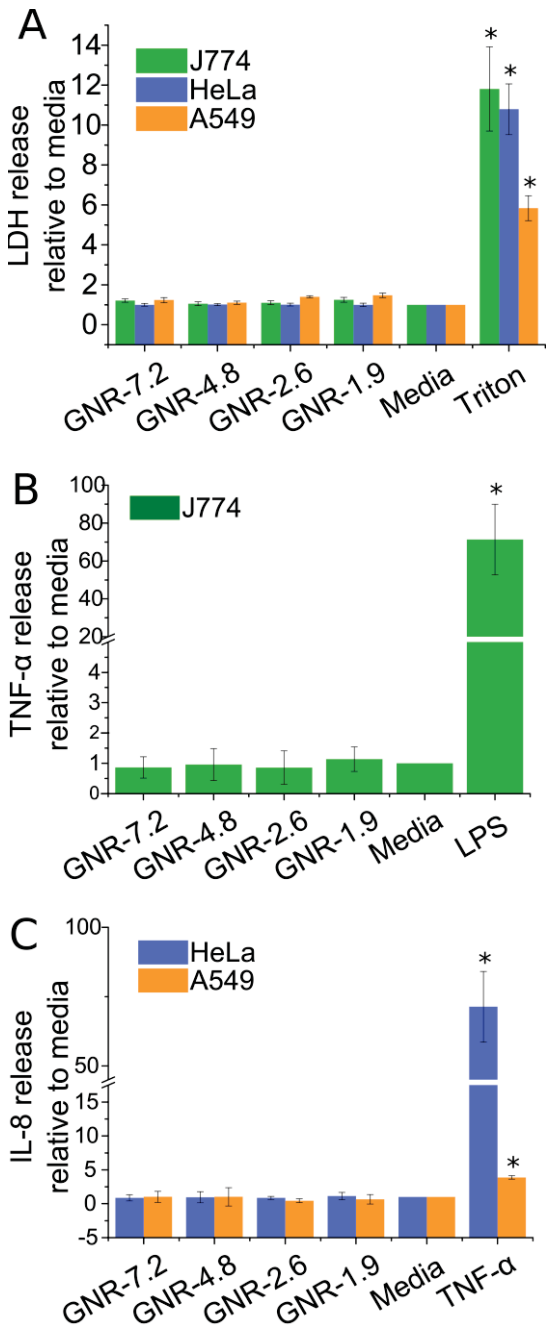

Fig. S7. Measurement of cytotoxicity and (pro-)inflammogenic potential of reshaped nanorods. (*A*) Cytotoxicity is expressed as a function of extracellular LDH after 24 h exposure to the reshaped GNRs (40 μg.mL^{-1}) relative to the negative control (considered as 1). Triton X-100, 0.2%, was used as the positive control. (*B*) Amount of extracellular TNF-α relative to negative control after 24 h exposure to the reshaped GNRs, with LPS

(100 ng.mL^{-1}) as the positive control. (*C*) Amount of extracellular IL-8 relative to negative control after 24 h exposure to the reshaped GNRs, with TNF-α (50 ng.mL^{-1}) as the positive control. Bars denote the mean ± SD, n=4. A two-way Tukey post-*hoc* ANOVA was performed and significance is indicated by: *p<0.05 against the negative control.

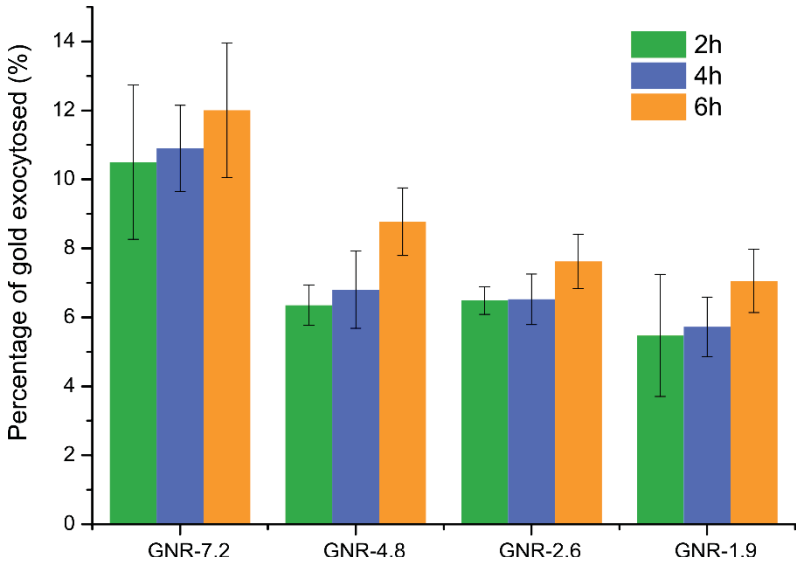

Fig. S8. Exocytosis of reshaped GNRs from HeLa cells. After an initial 24 h incubation with the reshaped GNRs (40 µg.mL^{-1}), the media was replaced with fresh supplemented RPMI and the exocytosed gold quantified by ICP-OES after 2, 4, or 6 h. The extracellular gold is expressed relative to the measured intracellular gold with bars denoting the mean ± SD, n=3.

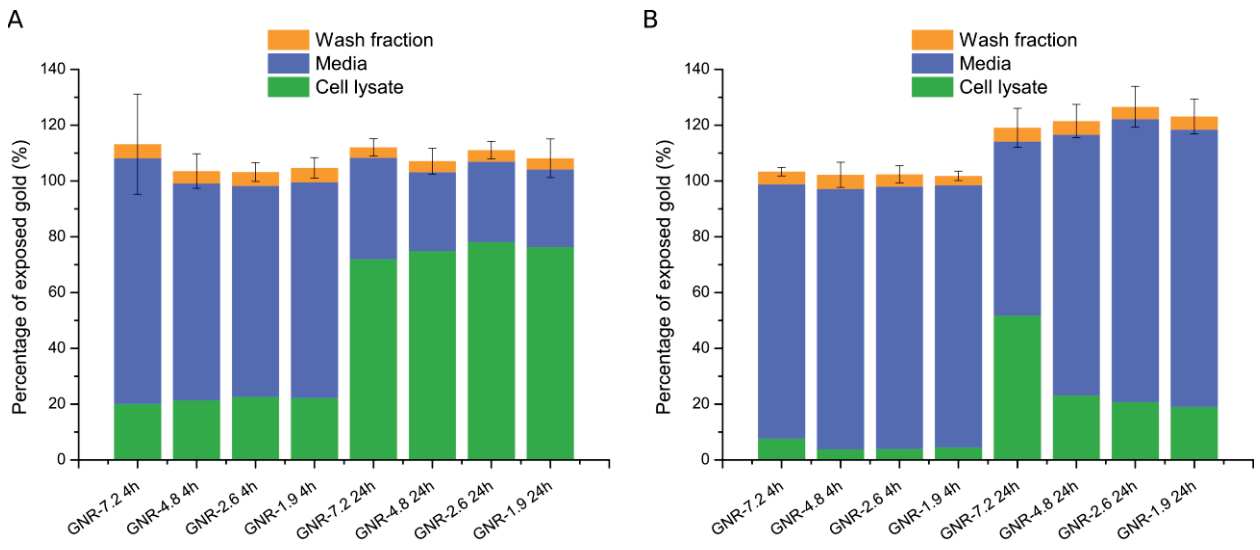

Fig. S9. Quantification of gold in different fractions. (*A*) J774A.1 cells and (*B*) HeLa cells incubated with reshaped GNRs (40 μg.mL^{-1}) for 4 h or 24 h. The cell lysate data is that of Figure 4, media corresponds to the quantity of gold that was not endocytosed, and wash fraction corresponds to the PBS and iodine washes which remove extracellular surface-bound GNRs. The data is expressed relative to the exposed quantity of GNRs, with bars denoting the mean ± SD, n=4.

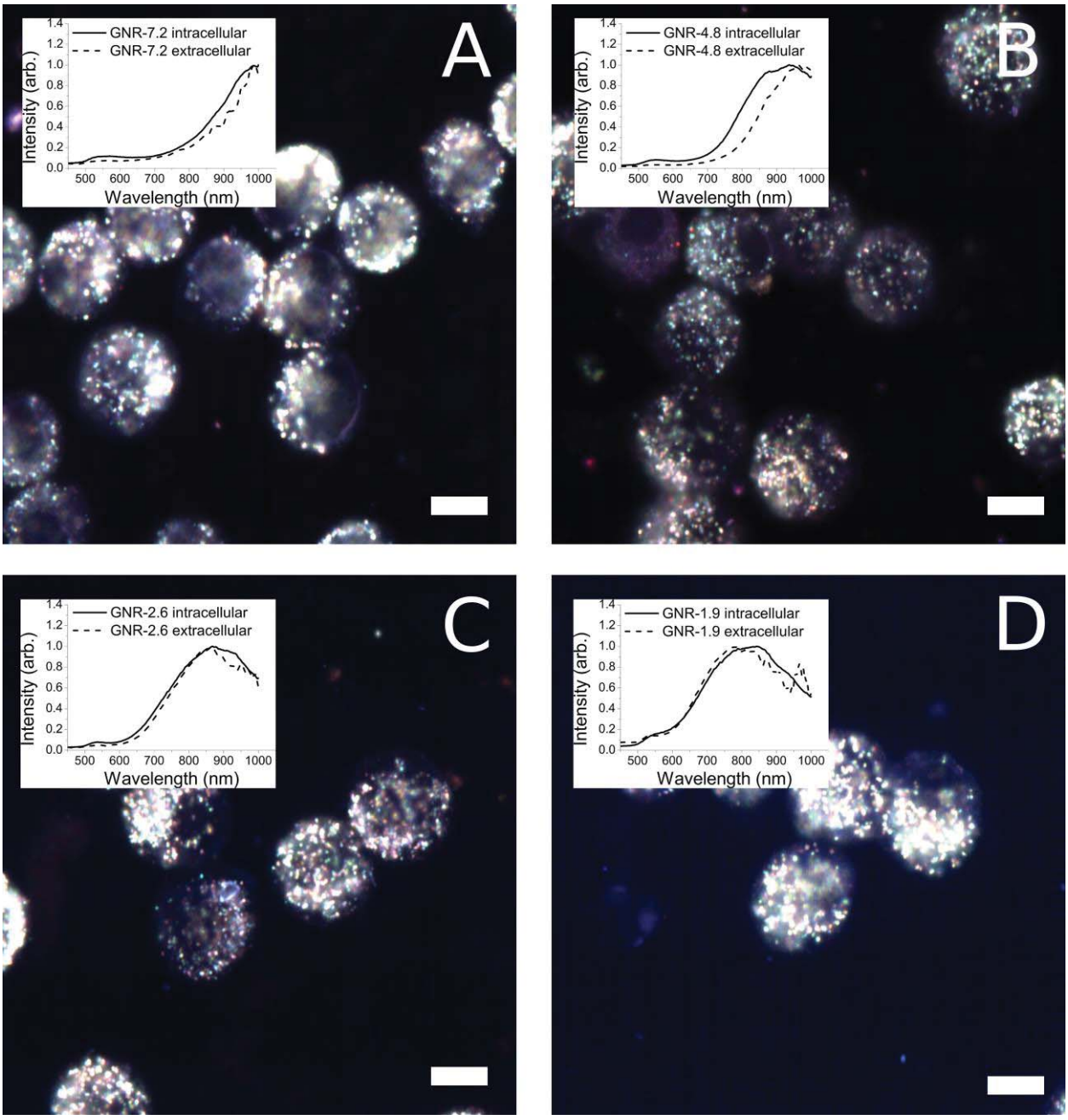

Fig. S10. Hyperspectral imaging combined with dark-field light microscopy of fixed and embedded J774A.1 cells. Exposed concentration of reshaped GNRs was 40 μg.mL^{-1} for 4 h: (*A*) GNR-7.2, (*B*) GNR-4.8, (*C*) GNR-2.6, and (*D*) GNR-1.9. Scale bar, 10 μm.

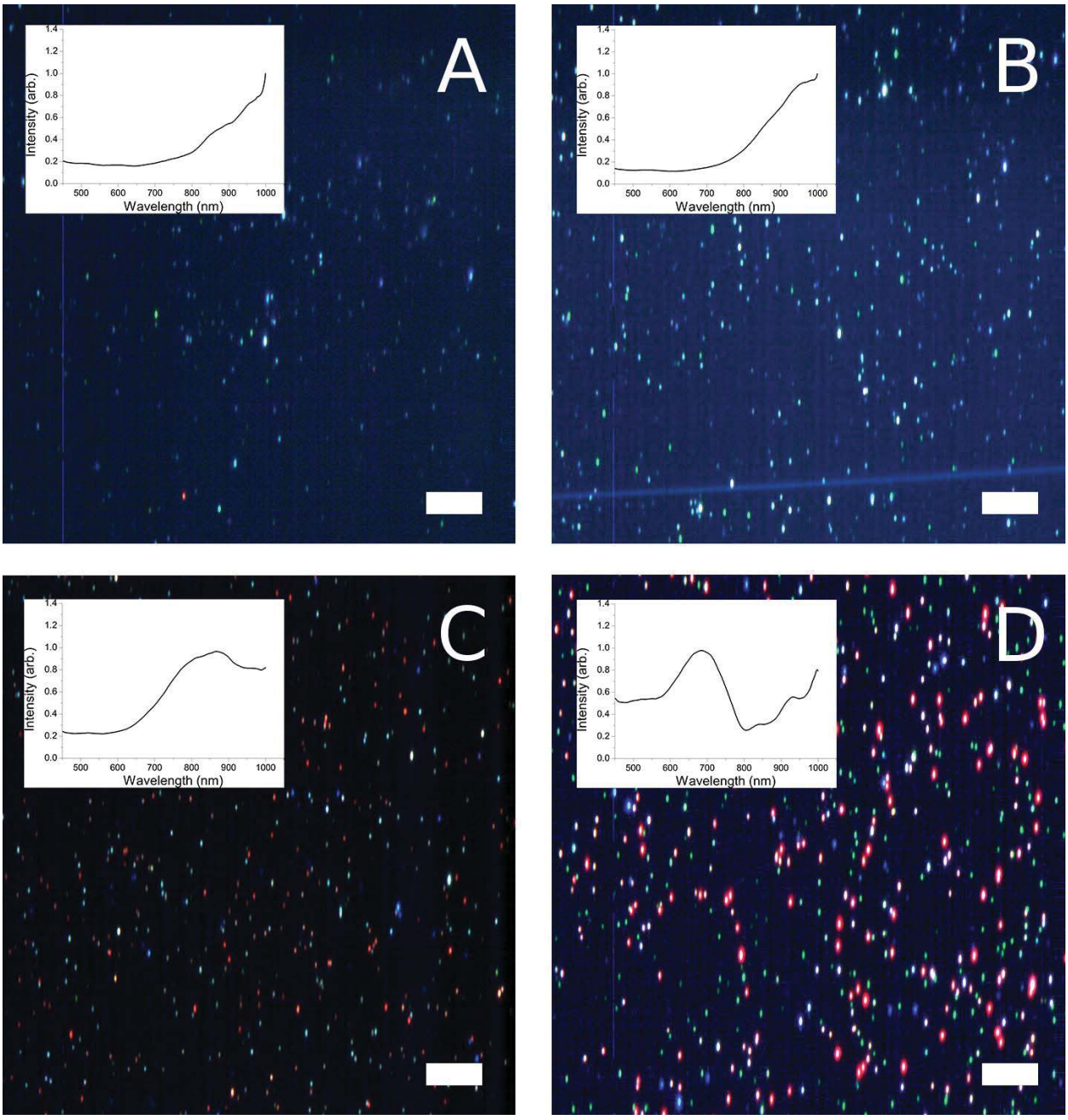

Fig. S11. Hyperspectral imaging combined with dark-field light microscopy of spin-coated GNRs. GNRs, 50 µL of 5 µg.mL^{-1}, in ethanol were spin-coated onto a glass slide: (*A*) GNR-7.2, (*B*) GNR-4.8, (*C*) GNR-2.6, and (*D*) GNR-1.9. Scale bar, 10 µm.

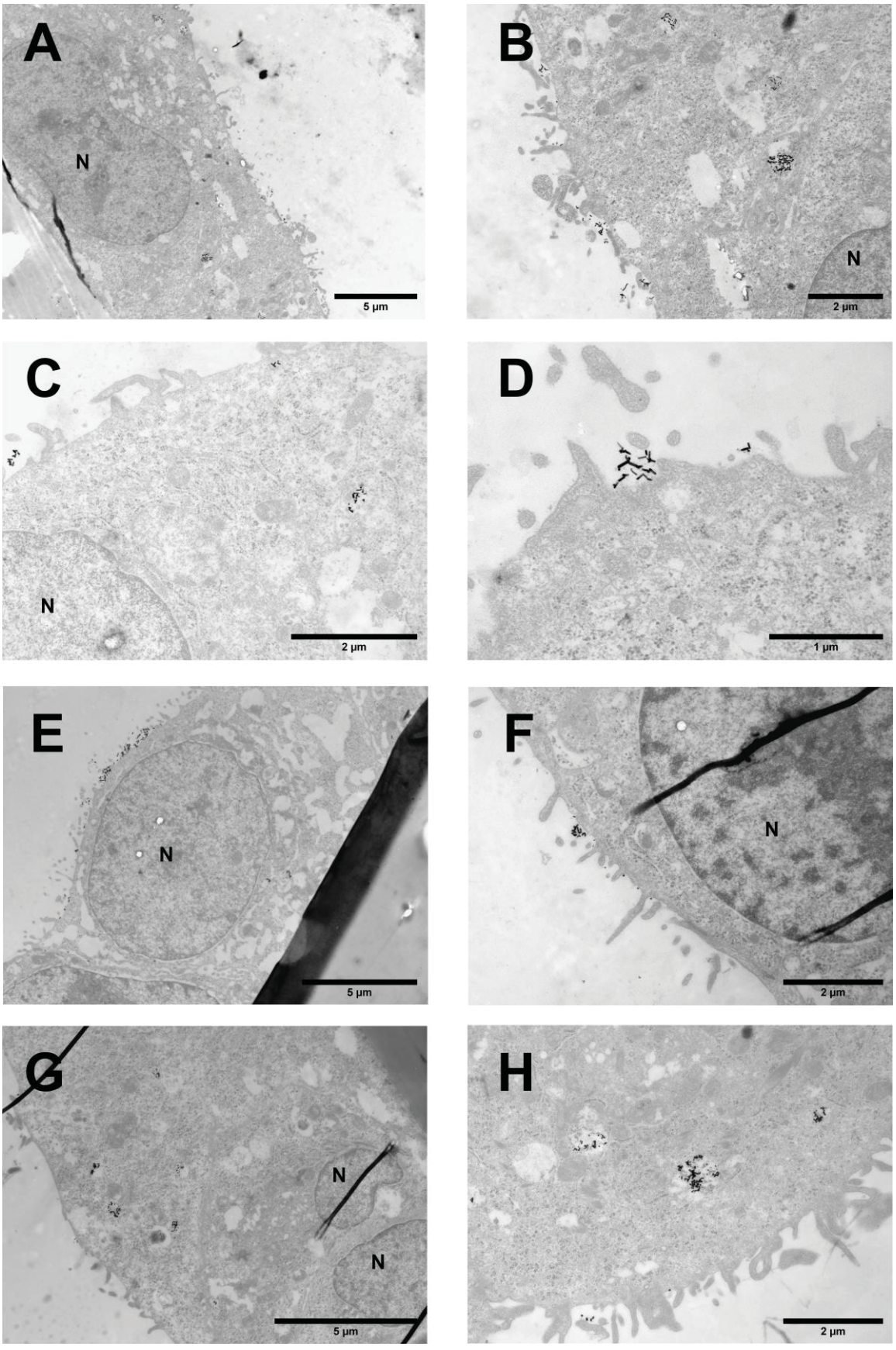
A
N
5 µm
B
N
2 µm
C
N
2 µm
D
1 µm
E
N
5 µm
F
N
2 µm
G
N
N
5 µm
H
2 µm

Fig. S12. TEM of A549 cells with intracellular GNRs. Representative TEM micrographs of embedded, stained, and sectioned A549 cells after incubation for 4 h with reshaped GNRs (40 μg.mL^{-1}): (*A*-*B*) GNR-7.2, (*C*-*D*) GNR-4.8, (*E*-*F*) GNR-2.6, and (*G*-*H*) GNR-1.9. The observed black lines in some of the images are artifacts caused by the cutting of two materials of different elasticity: the resin and the membrane.

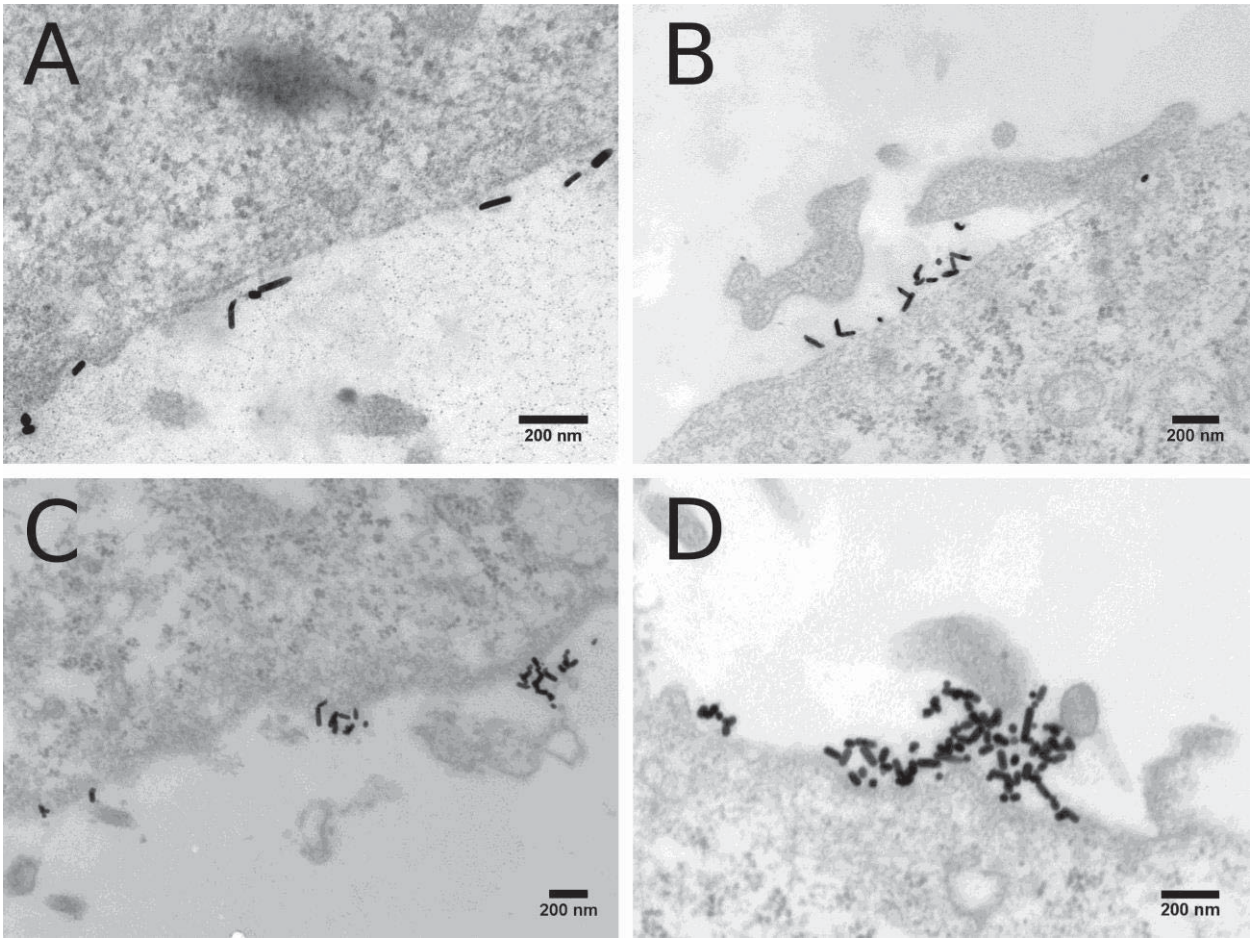

Fig. S13. Magnified TEM of A549 cells with intracellular GNRs. TEM micrographs of embedded, stained, and sectioned A549 cells after incubation for 4 h with reshaped GNRs (40 μg.mL^{-1}): (*A*) GNR-7.2, (*B*) GNR-4.8, (*C*) GNR-2.6, and (*D*) GNR-1.9.

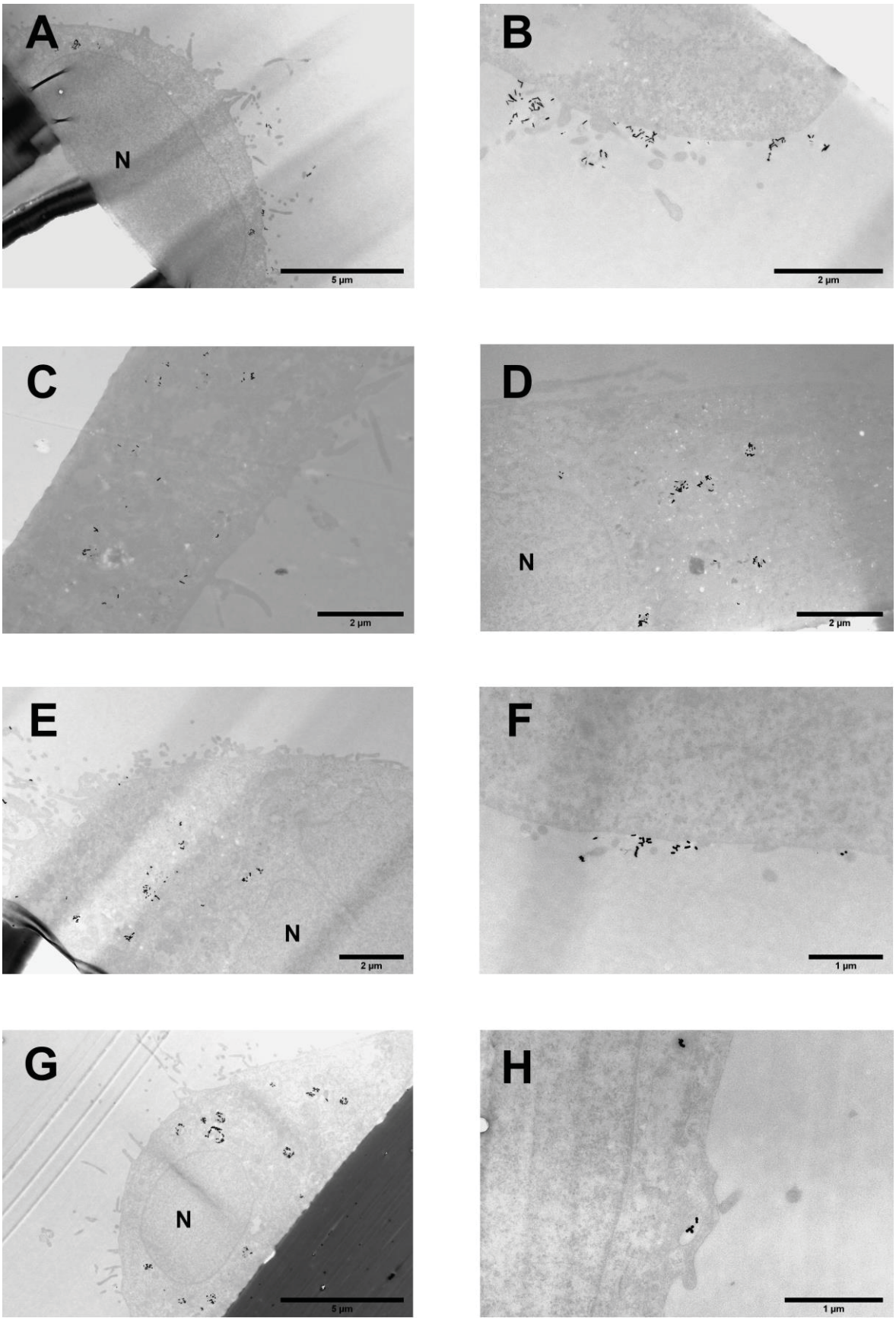
A
N
5 µm
B
2 µm
C
2 µm
D
N
2 µm
E
N
2 µm
F
1 µm
G
N
5 µm
H
1 µm

Fig. S14. TEM of HeLa cells with intracellular GNRs. Representative TEM micrographs of embedded, stained, and sectioned HeLa cells after incubation for 4 h with reshaped GNRs (40 μg.mL^{-1}): (*A*-*B*) GNR-7.2, (*C*-*D*) GNR-4.8, (*E*-*F*) GNR-2.6, and (*G*-*H*) GNR-1.9. The observed black lines in some of the images are artifacts caused by the cutting of two materials of different elasticity: the resin and the membrane.

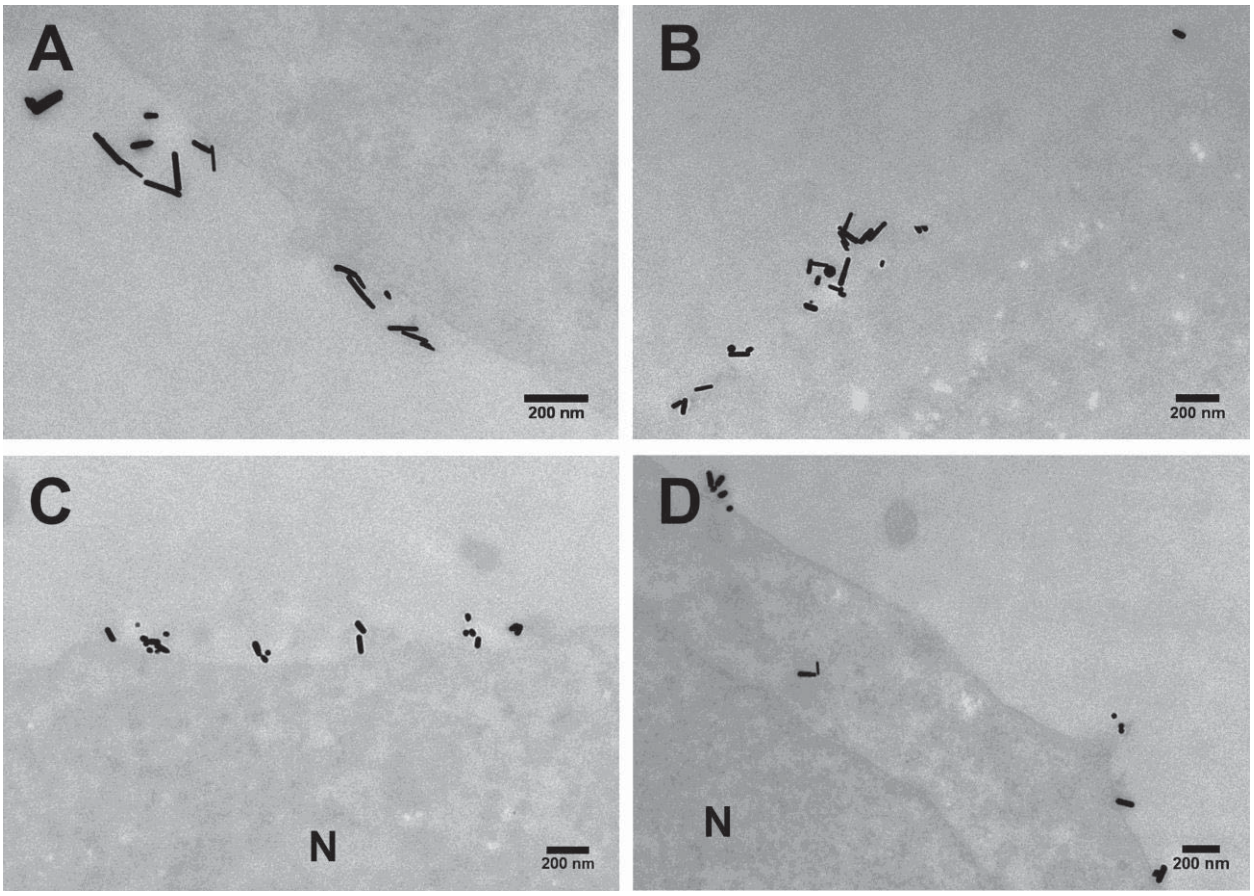

Fig. S15. Magnified TEM of HeLa cells with intracellular GNRs. TEM micrographs of embedded, stained, and sectioned HeLa cells after incubation for 4 h with reshaped GNRs (40 μg.mL^{-1}): (*A*) GNR-7.2, (*B*) GNR-4.8, (*C*) GNR-2.6, and (*D*) GNR-1.9.

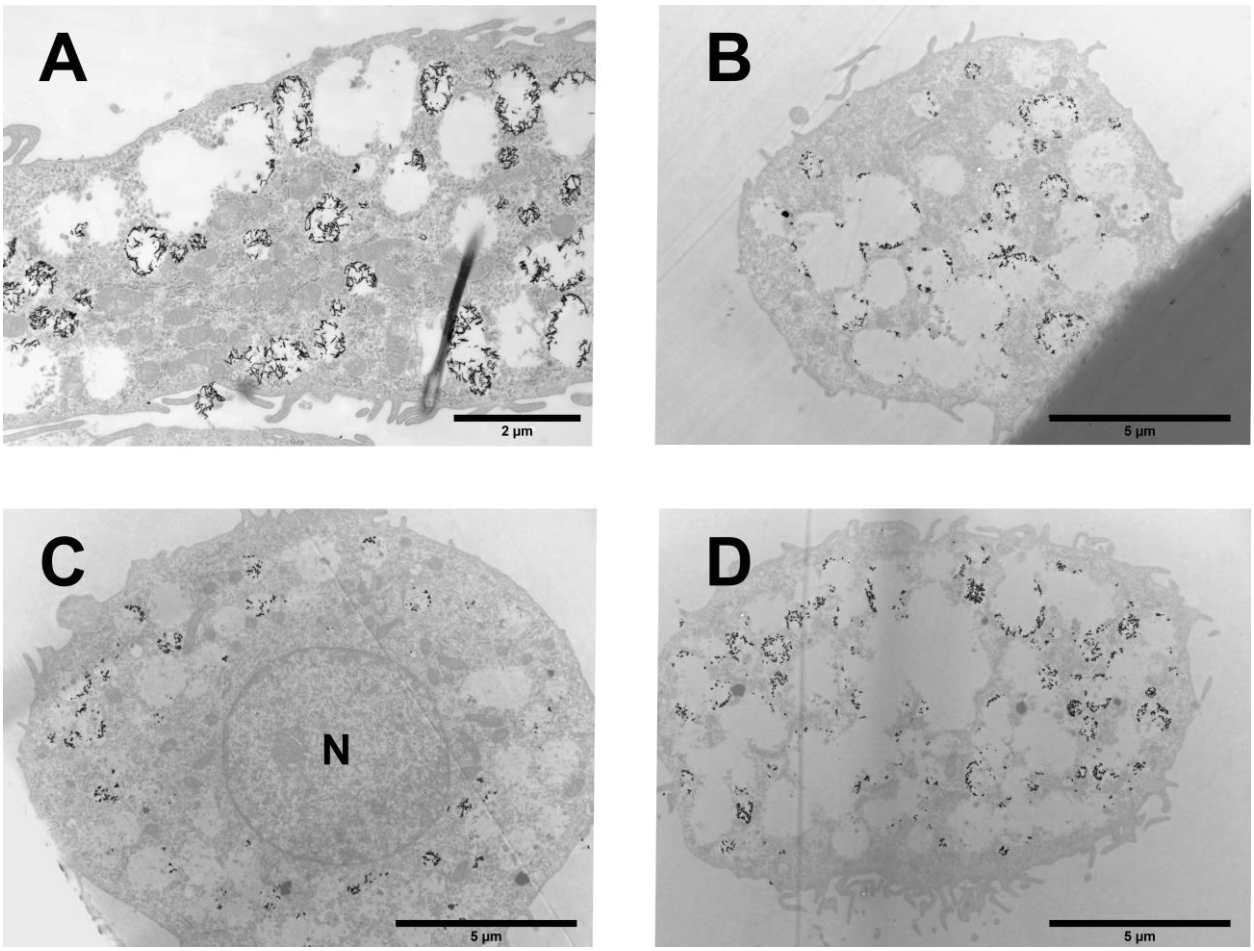

Fig. S16. TEM of J774A.1 cells with intracellular GNRs. Representative TEM micrographs of embedded, stained, and sectioned J774A.1 cells after incubation for 4 h with reshaped GNRs (40 µg.mL^{-1}): (*A*) GNR-7.2, (*B*) GNR-4.8, (*C*) GNR-2.6, and (*D*) GNR-1.9. The observed black line in (*A*) is an artifact caused by the cutting of two materials of different elasticity: the resin and the membrane.

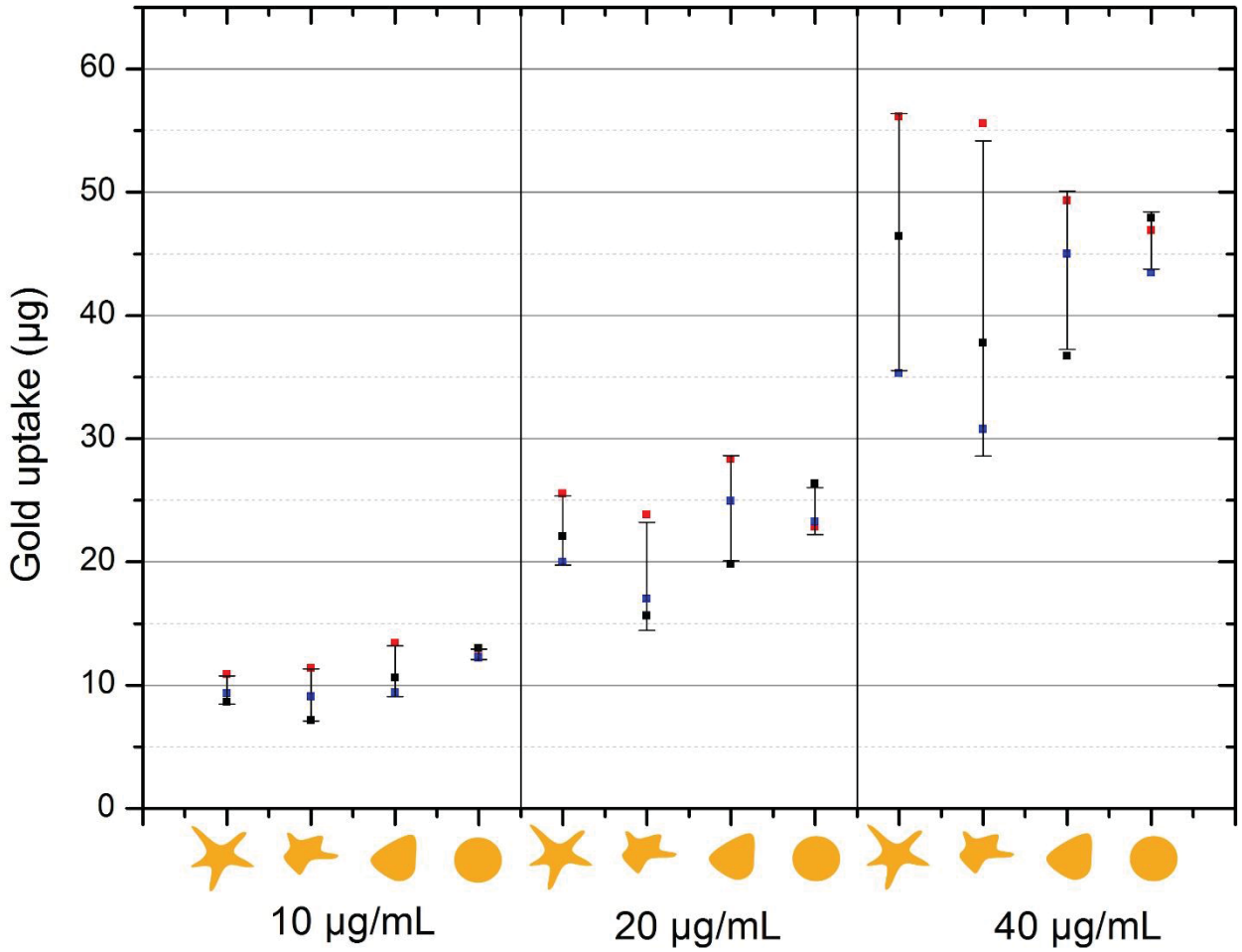

Fig. S17. Dose-response on uptake of reshaped gold nanostars. The reshaping protocol described below was applied to gold nanostars, which were then exposed to J774A.1 cells at three different concentrations (10, 20, and 40 µg/mL) for 24 h.